PRELIMINARY RESULTS ON HIGH ACCURACY ESTIMATION OF SHORELINE CHANGE RATE BASED ON COASTAL ELEVATION MODELS

F.J. Aguilar [a,*], I. Fernández [a], J.L. Pérez [b], A. López [a], M.A. Aguilar [a], A. Mozas [b], J. Cardenal [b]

[a] Dept. of Agricultural Engineering, Almería University, La Cañada de San Urbano s/n, 04120 Almería, Spain - (faguilar, ismaelf, maguilar)@ual.es

[b] Dept. of Cartographic Engineering, Geodesy and Photogrammetry, Jaén University, Las Lagunillas s/n, 23071 Jaén, Spain – (jlperez, alarenas, antmozas, jcardena)@ujaen.es

Commission VIII, WG9

KEY WORDS: Coast, Monitoring, Change detection, LIDAR, DEM/DTM, Mapping, Shoreline

ABSTRACT:

The shoreline is one of the most important features on the Earth's surface, representing a critical indicator of coastal evolution and vulnerability for any Coastal Geographic Information System. In this sense, a new methodological proposal for high accuracy shoreline mapping is outlined along the present work. Briefly, this methodology starts from a coastal elevation model (CEM) obtained by LiDAR or stereo-protogrammetric technologies and vertically geo-referenced to a geodetic datum. The second step would consist on mapping the contour line corresponding to the 0 m elevation to draw the continuous line that represents the physical intersection between land and the reference geoid, i.e. the Mean Sea Level (MSL). The problem is that most of time the boundary between water and land is not clear because LiDAR or stereo-photogrammetric data may be contaminated by waves and runup. So those data should be first eliminated by removing all of data points that lie seaward of that theoretical boundary. Then we suggest the use of extrapolation methods to cope with this problem, presenting and evaluating the performance of two algorithms for extrapolating the MSL contour line from CEMs. The first one is based on a classic approach named Cross-Shore Profile method where linear regression is computed along different cross-shore profiles to extrapolate the corresponding shoreline position as the intersection between the regressed straight line and the selected tidal datum. The second method is a new iterative grid-based data technique that expands the Elevation Gradient Trend computed for every grid point to extrapolated grid points with unknown heights. The process is repeated till the new grid point reaches the level just below the chosen tidal datum. After that, the border which separates grid points (above and below the reference height) is joined to map the corresponding tide-coordinated shoreline.
From the analysis of the obtained results, both quantitative and qualitative, the new grid-based approach can be strongly recommended because its precision, local slope acquisition, robustness regarding the presence of noise and outliers, and capability to deal with very curved and even closed coastal features. The preliminary results also indicate that, though the global rate-of-change for the whole coastline between 2001 and 2009 may be catalogued as relatively low (0.55 ± 0.50 m/year of net accretion), the local results for every one of the 29 homogeneous units considered have been extremely variable and statistically significant, ranging from 3.85 ± 0.61 m/year accretion to 3.97 ± 0.56 m/year erosion. In this way, many local phenomena, registered in a short-term period and mainly due to human intervention, may strongly affect the shoreline evolution in certain and localized areas.

1. INTRODUCTION

Coastal areas are one of the most dynamic and changing natural environments over the Earth surface. In addition, urban development on the coastal area and resource use conflicts spawn environmental degradation and increasing hazard vulnerability (Mills et al., 2005). These facts, joined to widely predicted Sea Level Rise (SLR) due to climate change, have encouraged the development of new and more precise methods for mapping shorelines evolution. Under this point of view, detailed coastal topographic information will be the key variable in understanding the likely impacts of SLR global natural hazard.
Since the 1920s, aerial photogrammetry has replaced more and more traditional ground surveys headed up to capture beach surface by means of topographic profiling. In recent decades, new technologies have arisen for coast and shoreline mapping, including high resolution satellite imagery, kinematic GPS vehicles and, above all, airborne LiDAR surveys (Brock and Purkis, 2009).
As it is widely known, a shoreline is defined as the theoretical line of contact between land and water, something easy to establish but very difficult to map because its dynamic nature and the fact that water level is continuously changing (Di et al., 2003). In this regards, shoreline shifts may be observed along a day due to tidal fluctuations, being especially large for steep slope beaches located at macrotidal areas.
The High Water Line (HWL) is the most often used shoreline indicator when it is interpreted in the field or from aerial photographs. From a practical point of view, HWL is generally identified as the wet/dry sand boundary following high tide (Robertson et al., 2004). In this sense, LiDAR surveys are quite efficient as compared with coastlines extracted from digital ortophotography or photo interpretation. That is because LiDAR-based shorelines are geo-referenced to a certain tidal datum which avoids problems related to biases or horizontal

* Corresponding author. This is useful to know for communication with the appropriate person in cases with more than one author.

shifts bound to the presence of different tidal levels when the images were taken or possible misinterpretations of the wet-dry beach line (Crowell et al., 1991). Hence using tidal datum indicators is a more objective way to identify the shoreline, although it requires counting on a high resolution Coastal Elevation Model (CEM), as accurate as possible, derived by means of stereo-photogrammetry, LiDAR or ground survey data (Gens, 2010).

Depending on the method to be used for extracting shoreline, the recommended time of data capture may be variable. For example, aerial photograph acquisitions are normally scheduled when surface water level is close to the Mean High Water (MHW) datum value for the working area whereas the optimal time for LiDAR surveys would be when most of the intertidal zone is exposed, i.e. near the time of Mean Lower Low Water (MLLW) datum value. It is needed to underline that MHW, that is the average of all the high water orthometric heights observed over the National Geodetic Vertical Datum, represents the legal shoreline datum in the United States. However, the elevation of the MHW tidal datum may experience large variations along the coast as a function of the local tide range and mean tide level. This is the main reason why an open coast tide station very close to our working coastal area is needed to accurately estimate its MHW. And it is not always available. Thus sometimes it is recommendable to use as a more reliable vertical reference the Mean Sea Level (MSL) tidal datum. For example, in Spain that vertical datum will take the geode as reference surface, adopting as null orthometric height point the medium level in the calm seas of Alicante. In fact, a reasonably dense geodetic network is actually available in Spain which allows to locally and accurately establish that vertical datum in everywhere along the Spanish coast.

The main goal of this work is to look for a response to all the commented shortcomings, outlining a new methodological proposal for high accuracy shoreline mapping based on CEMs processing. The extracted shoreline, including uncertainty computation, will be used to estimate shoreline rate-of-change for a pilot area and propose an integrated methodology to high accuracy estimation of shoreline change rate.

2. SHORELINE EXTRACTION METHODS

2.1 The classic approach: the Cross-Shore Profile method

The shoreline position computed from tidal datum surface geo-referenced CEMs has been previously afforded by the Cross-Shore Profile method (CSP). This technique fits a regression line to LiDAR or stereo-photogrammetrically captured points along foreshore profiles and afterwards calculates the intersection between that adjusted line and the chosen water level or tidal datum value (Stockdon et al., 2002; Morton et al., 2005). In doing so a number of shoreline points are estimated (one for every profile or transect) and are then linked to represent the corresponding shoreline (Fig. 1).

This work also contributes presenting a theoretical framework to estimate the point shoreline error propagated from CSP method. First of all, least squares estimation must be used to obtain the parameters a (slope) and b (intercept) of the computed regression line (functional equation z = ax + b). Starting from that computation, it is possible to obtain the corresponding variance-covariance matrix for the two estimated parameters $D_{a,b}$:

$$D_{a,b} = \begin{pmatrix} \sigma_a^2 & Cov_{a,b} \\ Cov_{a,b} & \sigma_b^2 \end{pmatrix} \quad (1)$$

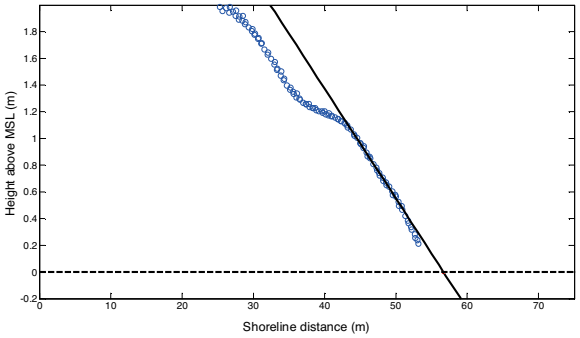

Figure 1. Cross-shore profile showing a very good adjustment to a straight line ($r^2 = 0.98$). Dash-line depicts MSL datum.

Now it is needed to calculate the uncertainty with regards to the intersection point (x_s) between the regression line and the considered tidal datum (e.g. MHW or MSL) given by:

$$\hat{x}_s = \frac{m - \hat{b}}{\hat{a}} \quad \text{and being } m = MHW \text{ or } MSL \quad (2)$$

Attending the general model for error propagation by Taylor series:

$$\sigma^2_{\text{xs regression}} = \sum_{i=1}^{2}\sum_{j=1}^{2} \rho_{i,j}\sigma_i\sigma_j \frac{\partial x_s}{\partial v_i}\frac{\partial x_s}{\partial v_j} \quad (3)$$

$$\text{with } v_i = a, v_j = b, \rho_{a,b} = \frac{Cov(a,b)}{\sigma_a\sigma_b}$$

Next the uncertainty for the x_s position due to the regression goodness-of-fit can be derived:

$$\sigma^2_{\text{xs regression}} = \frac{\sigma^2_a (m-\hat{b})^2}{\hat{a}^4} + \frac{\sigma^2_b}{\hat{a}^2} + 2\,Cov(a,b)\frac{(m-\hat{b})}{\hat{a}^3} \quad (4)$$

Now we have to sum the vertical uncertainty owing to the own error of data capture (standard deviation σ_z of LiDAR or stereo-photogrammetry derived CEM translated to planimetric error by means of σ_z/a) to the regression uncertainty given by equation 4, obtaining the following total uncertainty for the calculated x_s position (epsilon band):

$$\sigma_{xs} = \sqrt{\sigma^2_{xs\ regression} + \frac{\sigma_z^2}{\hat{a}^2}} \quad (5)$$

2.2 A new approach: the Elevation Gradient Trend Propagation method

The Elevation Gradient Trend Propagation method (EGTP) presented along this work is a new approach, alternative to CSP method, to map shorelines starting from high resolution CEMs. It is based on an iterative grid-based data technique that expands the elevation gradient trend (norm and direction) computed for every grid point to extrapolated grid points with unknown heights. The process is repeated till the new grid point reaches the level just below the chosen tidal datum. After that, it is easy to join the border which separates grid points situated above and below the reference height to map the corresponding tide-coordinated shoreline.

The algorithm starts from a high resolution grid CEM (e.g. 1 m grid size) to be extrapolated towards decreasing heights looking

for to reach the tidal datum. Previously the vector elevation gradient has to be computed by means of the known expression:

$$\vec{G} = \frac{\partial z}{\partial x}\vec{\mathrm{i}} + \frac{\partial z}{\partial y}\vec{\mathrm{j}} \tag{6}$$

Where the components for x and y directions are computed by applying a Sobel filter to the grid CEM using a 3x3 window:

$$\frac{\partial z}{\partial x} \cong Z \otimes \begin{bmatrix} -1 & 0 & 1 \\ -2 & 0 & 2 \\ -1 & 0 & 1 \end{bmatrix}; \frac{\partial z}{\partial y} \cong Z \otimes \begin{bmatrix} -1 & -2 & -1 \\ 0 & 0 & 0 \\ 1 & 2 & 1 \end{bmatrix} \tag{7}$$

First of all, a height threshold value has to be established to avoid CEM contamination due to noisy points on wave crests and run-up (points on the sea-land boundary). In this case, a conservative value of 40 cm was selected because, unfortunately, an approximated sea level of 18.5 cm above geodetic datum was estimated when the 2009 LiDAR survey was carried out. Thus all grid points presenting heights below 40 cm were removed to be later extrapolated.

It is worth to point out that, in every iteration, the elevation gradient for components x and y is only computed for those central grid points which present a complete neighborhood (i.e. all the 8 neighbours have a height value). The elevation gradient for each component of those grid points located at the border was interpolated by means of the inverse distance weighting method, using a local support made up of the gradients really calculated on the nearest adjacent grid points.

In a second step, and starting from the previosly computed gradient for x and y directions, it is necessary to extrapolate the unknown heights as it is depicted in Fig. 2. That iterative process must be continued till reaching the first negative values in the case we are searching for the MSL tidal datum.

Finally, the extrapolate height for the central pixel is accomplished by means of the following expression (see Fig. 2):

$$z_{extrapolated} = \frac{\sum_{\forall i,j} \left(z_{ij} + \mathrm{Gx}_{ij} \Delta j_{ij} + Gy_{ij} \Delta i_{ij} \right)}{C} \tag{8}$$

Where i and j refers to those cells in the reference window (matrix M) presenting a height value different than 0 and C is the number of cells used for height propagation.

In this case, the shoreline position uncertainty is obtained in two steps. First, the vertical uncertainty for every grid point is derived from two components (Aguilar et al., 2010):

$$\sigma^2_{total} = \sigma^2_{CEM} + \sigma^2_{\text{propagation}} \tag{9}$$

Being σ^2_{CEM} the original CEM vertical accuracy (σ_z) previously calculated from a set of adequate and highly accurate check points. $\sigma^2_{propagation}$ is the vertical error propagated from EGTP extrapolation method.

Initial gradient components Gx_0 and Gy_0 can be written as follows for every grid point presenting a full neighbourhood (From Sobel filter application as described in eq. 7):

$$\mathrm{Gx}_0 = \frac{z_{13} - z_{11} + 2(z_{23} - z_{21}) + z_{33} - z_{31}}{4.2.\Delta x} \tag{10}$$

$$\mathrm{Gy}_0 = \frac{z_{13} - z_{11} + 2(z_{23} - z_{21}) + z_{33} - z_{31}}{4.2.\Delta y}$$

Being Δx and Δy the grid spacing along the directions x and y ($\Delta x = \Delta y = 1$ m in our case). Applying the error propagation theory to equation 10, the next expression can be drawn:

$$\sigma^2_{\mathrm{Gx}_0} = \frac{3.\sigma_z^2}{16.\Delta x^2};\ \sigma^2_{\mathrm{Gy}_0} = \frac{3.\sigma_z^2}{16.\Delta y^2} \tag{11}$$

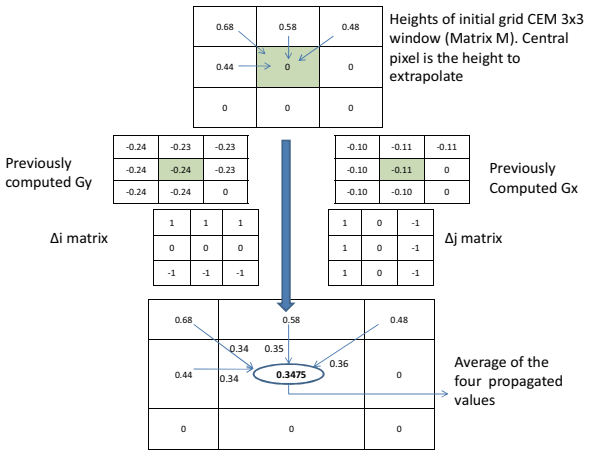

Figure 2. Algorithm used to propagate the CEM heights from the application of previously computed gradient x and y.

Now, this previous gradient error has to be propagated to unknown cells taking into account the interpolation method used to fill in the boundaries, i.e. inverse distance weighting in this case (the same could be written for component Gy):

$$\sigma^2_{\mathrm{Gx\ propagated}} = \frac{1}{\left(\sum_{i=1}^{N} \frac{1}{d_i} \right)^2} \left(\sum_{i=1}^{N} \sigma^2_{z_i} / d_i^2 \right) \tag{12}$$

N would be the number of neighbours presenting a gradient value within the 3x3 window surrounding the central pixel. The d_i values are representing distance between grid points.

Therefore the total gradient error for every grid point could be attained (the same would be applicable to Gy):

$$\sigma^2_{Gxtotal} = \sigma^2_{Gx_0} + \sigma^2_{\mathrm{Gx\ propagated}} \tag{13}$$

Notice that the gradient error will be increased after each iteration because the growing uncertainties of extrapolated heights.

Eq. 14 shows how to propagate the vertical error due to total gradient error and central window height extrapolation using Eq. 8 as reference. It is worth to point out like grid spacing effectively affects the uncertainty of extrapolated height so it is strongly recommended to use high resolution CEMs.

$$\sigma^2_{z\ \mathrm{propagated}} = \frac{\sum_{\forall i,j} \left(\sigma^2_{z_{ij}} + \sigma^2_{Gx\ total_{ij}} .\Delta x^2 + \sigma^2_{Gy\ total_{ij}} .\Delta y^2 \right)}{C^2} \tag{14}$$

The initial CEM vertical error has to be added to the propagated one to estimate the total vertical accuracy for extrapolated grid points (see Eq. 9):

$$\sigma^2_{z\ \mathrm{total}} = \sigma^2_{z\ \mathrm{propagated}} + \sigma^2_{z\ CEM} \tag{15}$$

Finally, and as the second and last step, vertical error has to be translated to planimetric one to obtain the shoreline position uncertainty. For it, let us suppose that two points A and B, presenting positive and negative heights respectively, have been indentified and linear interpolation is afforded to estimated the 0 m height (MSL tidal datum) shoreline point x_s. The following expressions can be easily deduced:

$$slope = \frac{z_B - z_A}{d_{AB}};\ d_{A0} \approx x_s = \frac{-z_A}{slope} \qquad (16)$$

$$\sigma^2_{slope} = \frac{1}{d^2_{AB}}\left(\sigma^2_{z_A} + \sigma^2_{z_B}\right);\ \sigma_{A0} \approx \sigma_{xs} = \sqrt{\frac{\sigma^2_{z_A}}{slope^2} + \frac{\sigma^2_{slope} z^2_A}{slope^4}}$$

3. STUDY SITE, DATASETS AND METHODOLOGY

3.1 Study Site

The previously described shoreline mapping methods were tested on two CEMs comprising a heavily developed coastal area of Almería (Mediterranean Sea, South Spain) around 11 Km long and taken the years 2001 and 2009. The working area was concretely situated between the harbours of Garrucha and Villaricos. It would be a typical study on short-term shoreline dynamics which is usually carried out at small spatial scales during a time span of less than 10 years (Crowell et al., 1993). The vertical reference datum (null orthometric height point or level 0 m) was the medium level in the calm seas of Alicante (Spain), the official vertical datum for orthometric elevations in Spain. The average slope along the whole coastline was estimated as 13% as the average of 2001 and 2009 computed slopes.

3.2 Datasets

3.2.1. Data corresponding to 2001: Come from an analogic RGB photogrammetric flight at an approximated scale of 1:5000 taken on 9 April 2001. 1 m grid-spacing CEM was carried out by means of stereo matching techniques ranking over previously digitized images and subsequent exhaustive and careful edition by one operator. SOCET SET® 5.4 environment was used to complete the whole photogrammetric digital flow. The estimated vertical accuracy of the photogrammetrically-derived CEM was around 30 cm. On the other hand, the stereovision capabilities of that system allowed to estimate the mean sea level at time when photographs were taken, obtaining an average orthometric height around 1.4 cm, that is very near MSL tidal datum.

3.2.2. Data corresponding to 2009: The CEM corresponding to 2009 (28 August) was a high accuracy and resolution LiDAR-derived CEM. The flight height above ground was about 1000 m, using a Leica ALS60 airborne laser scanner with 35º FOV, 1.61 points/m^2 average point density and counting on two ground GPS reference stations. The estimated vertical accuracy computed from 62 DGPS high accuracy check points distributed over the whole working area showed a vertical accuracy (measured as standard deviation) of 8.9 cm. All the processes to filter the laser point cloud, adjusting the four flight-lines strips and managing LiDAR data were carried out by means of TerraMatch® and TerraScan® 010.
In this case TerraScan® software also allowed estimating the mean sea level by plane-to-cloud adjustment at time when LiDAR data were taken, turning out to be around 18 cm average in open coast. That is very near the locally corrected MHW estimated from historical data coming from the tide gauge station located at Almería harbour (non open coast station), which would take a value around 20 cm.

3.3 Shoreline rate-of-change computation and statistical analysis

All methods used for calculating shoreline rates-of-change involve measuring the differences between shoreline positions through time. Although there are very sophisticated methods to be used in the case of counting on more than two shoreline positions (see Genz et al., 2007 for instance), the simplest method called End Point Rate (EPR) has been used in this work because only two shoreline positions were available.
The Digital Shoreline Analysis System (DSAS) software from U.S Geological Survey allowed computing rate-of-change (m/year) between 2001 and 2009 through the MSL and MHW shorelines vector data by applying the Single Transects method (Thieler et al., 2009).
Because we have previously estimated the uncertainty corresponding to each shoreline point, it is now possible to compute the statistical significance for each EPR value calculated along a certain transect and statistically accept or not whether it is really reporting erosion or accretion at that foreshore point. Let us suppose that shoreline position for certain transect in 2001 is a random variable A and another random variable B in 2009. Knowing that the t statistics follows a t-Student distribution (Eq. 17) and that the null hypothesis establishes $\mu_A = \mu_B$, so $\mu_d = 0$, t values greater than 1.96 (95% confidence level) should be obtained to statistically assure that the computed EPR is different to 0 m/year, that is a non casual change has been registered. On the contrary, t values below 1.96 means no change has been registered, hence that particular EPR value was set up to 0 m/year in the subsequent analysis.

$$t = \frac{\hat{d} - \mu_d}{\sigma_d};\ \hat{d} = Xs_B - Xs_A;\ \sigma_d = \sqrt{\sigma^2_{Xs_A} + \sigma^2_{Xs_B}} \qquad (17)$$

$$H_0 : \mu_A = \mu_B \Rightarrow \mu_d = 0 \Rightarrow \frac{\hat{d}}{\sigma_d} > t_{\alpha=0.05} \Rightarrow \mu_A \neq \mu_B$$

Finally, the EPR uncertainty, transect by transect, could be estimated by means of the next equation, where T represents the number of years passed between events A and B:

$$\sigma_{EPR} = \sqrt{\frac{\sigma^2_{Xs_A} + \sigma^2_{Xs_B}}{T^2}} \qquad (18)$$

Afterwards the EPR calculation, a full factorial design was deployed to search on the effects of different variables on the EPR experimental results. In this sense, we explored some sources of variation such as shoreline mapping method (CSP and EGTP), tidal datum (MSL = 0 cm and MHW = 20 cm), transect spacing (5, 10 and 20 m) and zones (29 homogeneous zones along the coastline qualitatively showing net erosion or accretion). An analysis of variance (ANOVA) was carried out using the EPR as observed variable and the mentioned factors (including the interactions between all those factors).

4. RESULTS AND DISCUSSION

4.1 Shoreline Estimated Uncertainty: Average MSL tide-coordinated shoreline uncertainties for the two tested methods presented in section 2, measured as standard deviations, are depicted in Table 1. It is necessary to stress that

CSP method showed a higher percentage of transects lost, i.e. a filtering process had to be arranged to remove very abnormal values due to poor adjustment (r^2<0.70, see Fig. 3), few points to adjust (<5) and/or extremely flat beaches (slope<0.02) presenting an intersection points x_s excessively away from the foreshore. In fact, this method seems to be quite sensitive to noise due to an incorrect separation between water and land, unexpected artifacts along foreshore profile or actually non-straight profiles. That is why there was a need to establish a suitable range of elevation data to avoid incorporating points above wave crests and run-up contamination in the wet beach area. In our case, and due to the high tide level registered in 2009 when LiDAR data were captured (see section 3.2.2), an elevation range between 0.4 and 0.8 m and a buffer area 2 m both sides of each transect were employed after an error-proof process.

On the other hand, EGTP can be deemed as much more robust than CSP, maintaining a greater number of useful transects. In this second case, the widely known 3 sigma rule was applied to remove some clear outliers due to excessively flat beaches.

The uncertainties obtained by means of airborne LiDAR data are similar (<1.5 m) than those reported by Stockdon et al. (2002), meanwhile photogrammetric-derived data registered a poorer estimated accuracy. Thus the final shoreline mapping accuracies are quite sensitive to the vertical accuracy of input data. Regarding the EGTP method, it is necessary to bear in mind that slightly higher uncertainties have been drawn because the need to establish a high vertical threshold (0.4 m) to filter out points above wave crests and runup contamination. Therefore higher number of iterations was needed to reach MSL tidal datum.

Year	Transects lost		Uncertainty (σ_{xs})	
	CSP	EGTP	CSP	EGTP
2001	12.84%	3.19%	2.95	4.10 m
2009	12.18%	1.54%	1.05 m	1.48 m

Table 1. Shoreline estimated uncertainty (MSL datum) for CSP and EGTP. Transects lost indicates the profiles not included for computation because presenting abnormal uncertainties.

4.2 Qualitative Analysis: It has dealt with a qualitative interpretation of the shoreline points. Regarding CSP method, and despite choosing a conservative vertical range of data described in section 4.4.1, some transects showed poor fit due to a wrong removal of points on water and/or actual beach profiles far away from a straight line (Fig. 3).

Furthermore, CSP method has shown irregular results depending on the coastline shape. For instance, curved and complex coastlines provoked unexpected wrong results regarding shoreline mapping. Equally, CSP is more sensitive than EGTP method to the presence of noise and outliers (crest-waves surge and runup, very flat beach, etc.), as can be observed in Fig. 4. Notice how some CSP computed shoreline positions in 2009 have been pointed far away from the actual shoreline. In this way, the EGTP method can be clearly considered as much more automatic, robust and predictable than the classic CSP method. As a general rule, EGTP method needn't any manual control or supervision, resulting in a fully unattended process very robust and adapted to work on winding coastlines.

4.3 Quantitative Analysis: Principal causes of coastal erosion or accretion, working on shore-term shoreline dynamics, are related to large storm events, seasonal variability in wave energy and/or circulation in the nearshore zone. Furthermore, and above all in heavily developed coastal areas presenting a high pressure owing to uncontrolled human activities, anthropogenic alterations may change processes of sediment supply and transport to sea, disrupting the natural shoreline evolution.

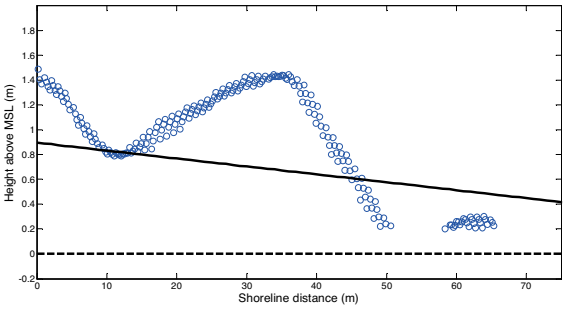

Figure 3. Cross-shore profile (CSP method) showing poor adjustment to a straight line (r^2 = 0.33). Dash-line means MSL datum. Notice a wave crest on the right.

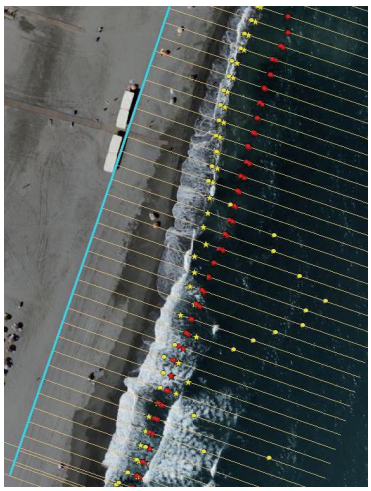

Figure 4. Orthophoto (images from year 2009) corresponding to zone number 25. Red color = 2001. Yellow color = 2009. Stars denote EGTP method and circles CSP method.

Other anthropogenic activities affecting shoreline evolution may be the presence of new engineered structures and artificial beach regeneration. In fact, the factorial ANOVA analysis has allowed stating that the variability between homogeneous units along the coastline is the main source of variation (factor D in Table 2) that can explain the most part of variability of the observed variable shoreline rate-of-change. Those variations are basically explained by the presence of artificial barriers such as breakwaters, harbors, dykes, etc., disturbing the long-shore continuity of coastline and producing micro-scale clusters showing net erosion or accretion. Neither shoreline mapping method nor tidal datum showed statistically significant effects on the variability of EPR experimental values. The same can be said about the three transect spacing tested (Table 2). Thus the definitive shoreline rate-of-change was computed using MSL tidal datum and 10 m transect spacing.

It is worth noting that significant effects (p<0.05) on rate-of-change were highlighted due to Method (A) by Zone (D) and Tidal Datum (B) by Zone (D) interactions. This is suggesting

that the shoreline mapping method and/or the selected tidal datum may produce significantly different results depending on the zones where they are applied, then confirming that shoreline evolution can be deemed as a very complex micro-scale based process when it has been polluted by anthropogenic activities.

Source of variation	Degrees freedom	Sum of squares	F	Signific. (p<0.05)
Method (A)	1	0.659	0.853	0.355
Tidal datum (B)	1	0.037	0.048	0.826
Transect spacing (C)	2	1.073	0.694	0.499
Zone (D)	28	33809.29	1562.34	**<0.001***
A*B	1	0.134	0.174	0.676
A*C	2	0.834	0.539	0.582
B*C	2	0.085	0.055	0.946
A*B*C	2	0.0292	0.037	0.962
A*D	25	66.756	3.455	**<0.001***
B*D	28	49.099	2.268	**<0.001***
A*B*D	25	9.991	0.517	0.977
C*D	56	41.945	0.969	0.540
A*C*D	47	5.744	0.158	1
B*C*D	56	1.802	0.041	1
A*B*C*D	47	1.003	0.0.027	1
Error	12412	9592.72		

Table 2. ANOVA table. Observed variable: rate-of-change 2001 to 2009. (*) Significant at 95% confidence level.

5. CONCLUSIONS

From the analysis of the obtained results, the new grid-based approach can be strongly recommended because its precision, local slope acquisition, robustness regarding the presence of noise and outliers, and capability to deal with very curved and even closed coastal features. The preliminary results also indicate that, though the global rate-of-change for the whole coastline between 2001 and 2009 may be catalogued as relatively low (0.55 ± 0.50 m/year of net accretion), the local results for every one of the 29 homogeneous units considered have been extremely variable and statistically significant, ranging from 3.85 ± 0.61 m/year accretion to 3.97 ± 0.56 m/year erosion. In this way, many local phenomena, registered in a short-term period and mainly due to human activities such as the presence of new engineered structures and artificial beach regeneration (the latter very intense and well documented along "Quitapellejos" beach), may strongly affect the shoreline evolution in certain and localized areas. Although not presented along this work because of space reasons, we would like to underline that classic High Water Line method over high resolution ortophotos from 2001 and 2009 was also applied, just as a reference, yielding an average rate-of-change of around 0.48 m of net erosion, clearly a wrong value. This fact confirms the bias introduced by the HWL method, erosion bias in our case, when it is applied over data coming from different tide conditions.

6. ACKNOWLEDGEMENTS

The authors are very grateful to Andalusia Regional Government, Spain, for financing this work through the Excellence Research Project RNM-3575 "Multisource geospatial data integration and mining for the monitoring and modelling of coastal areas evolution and vulnerability. Application to a pilot area located at Levante de Almería, Spain".

7. REFERENCES

Aguilar, F.J., Mills, J.P., Delgado, J., Aguilar, M.A., Negreiros, J.G., Pérez, J.L., 2010. Modelling vertical error in LiDAR-derived digital elevation models. *ISPRS Journal of Photogrammetry and Remote Sensing*, 65(1), pp. 103-110.

Brock, J.C., Purkis, S.J., 2009. The emerging role of Lidar remote sensing in coastal research and resource management. *Journal of Coastal Research*, 53, pp. 1-5.

Crowell, M., Leatherman, S.P., Buckley, M.K., 1991. Historical shoreline change: Error analysis and mapping accuracy. *Journal of Coastal Research*, 7(3), pp. 839-852.

Crowell, M., Leatherman, S.P., Buckley, M., 1993. Shore-line change rate analysis: long term versus short term data. *Shore and Beach*, 61(2), pp. 13-20.

Di, K., Ma, R., Li, R., 2003, Geometric processing of Ikonos stereo imagery for coastal mapping applications. *Photogrammetric Engineering and Remote Sensing*, 69(8), pp. 873-879.

Gens, R., 2010. Remote sensing of coastlines: detection, extraction and monitoring. *International Journal of Remote Sensing,* 31(7), pp. 1819-1836.

Genz, A.S., Fletcher, C.H., Dunn, R.A., Frazer, L.N., Rooney, J.J., 2007. The predictive accuracy of shoreline change rate methods and alongshore beach variation on Maui, Hawaii. *Journal of Coastal Research*, 23(1), pp. 87-105.

Mills, J.P., Buckley, S.J., Mitchell, H.L., Clarke, P.J., Edwards, S. J. (2005). A geomatics data integration technique for coastal change monitoring. *Earth Surface Processes and Landforms*, 30, pp. 651–664.

Morton, R.A., Miller, T., Moore, L., 2005. Historical shoreline changes along the US Gulf of Mexico: a summary of recent shoreline comparisons and analyses. *Journal of Coastal Research*, 21(4), pp. 704-709.

Robertson, W., Whitman, D., Zhang, K., Leatherman, S.P., 2004. Mapping shoreline position using airborne laser altimetry. *Journal of Coastal Research*, 20(3), pp. 884-892.

Thieler, E.R., Himmelstoss, E.A., Zichichi, J.L., Ergul, Ayhan, 2009. U.S. Geological Survey Open-File Report 2008-1278 "Digital Shoreline Analysis System (DSAS) version 4.0. An ArcGIS extension for calculating shoreline change", Woods Hole, MA, U.S. http://pubs.usgs.gov/of/2008/1278/ (accessed 16 May 2010).

Stockdon, H.F., Sallenger, A.H., List, J.H., Holman, R.A., 2002. Estimation of shoreline position and change using airborne topographic Lidar data. Journal of Coastal Research, 18(3), pp. 502-513.